International Journal of Thermal Sciences 209 (2025) 109549

Contents lists available at ScienceDirect

International Journal of Thermal Sciences

journal homepage: www.elsevier.com/locate/ijts

Effect of loaded carbon-based nanoparticles on the evaporation dynamics of sessile droplets

Zhihao Zhang , Yuying Yan *

Faculty of Engineering, University of Nottingham, University Park, Nottingham, UK

A R T I C L E I N F O

Keywords:
Droplet evaporation
Multi-walled carbon nanotubes
Multi-layer graphene
Coffee-ring effect

A B S T R A C T

Droplet evaporation is an essential physical process in industrial fields such as spray cooling and inkjet printing. With the widespread use of carbon materials, carbon-based nanofluid droplets have great potential to improve the efficiency and quality of applications in these fields. Therefore, understanding the effects of materials and external factors on the carbon-based nanofluid droplets evaporation dynamics becomes crucial. In this experimental study, the nanofluid droplets were prepared based on two common carbon-based nanomaterials, multi-walled carbon nanotubes (MWCNTs) and multi-layer graphene (MLG). The monocrystalline silicon wafer is used as the substrate, and the substrate temperature is controlled between 50 °C and 80 °C. Using the DI water droplets as a comparison, the effects of loading different carbon-based nanoparticles on wettability, evaporation modes, and heat transfer processes at the liquid-vapour interface were explored. The experimental results show that droplets loaded with MLG nanoparticles and sodium dodecyl sulfate (SDS) have the best evaporation efficiency, which can be improved by up to about 2.1 times compared with DI water. Furthermore, compared with the variable evaporation mode of the DI water droplets, the evaporation process of MLG nanofluid droplets is dominated by constant contact radius mode. At the same time, compared with DI water and MWCNTs, loaded MLG can reduce the liquid-vapour interface temperature difference by up to 3.7 °C and 1.0 °C, respectively, which effectively suppresses the evaporative cooling effect. Besides, the experimental results about the sedimentary pattern showed that MWCNTs can suppress the coffee-ring effect more effectively than MLG. Under various conditions, MLG nanoparticles can make the sedimentary pattern have greater surface roughness, which is about 1.8 times higher on average compared with MWCNTs.

1. Introduction

Carbon-based materials mainly refer to materials with carbon as the main body, among which high-performance materials such as graphene and carbon nanotubes have been widely used in industrial production and scientific research [1,2], such as high-heat-flux devices cooling [3], nano fuel [4], bacteria detection [5], and integrated circuit fabrication [6]. Among them, the thermal management of electronic devices has emerged as an essential issue in modern life. Several cooling methods have been developed to achieve this [7], of which direct cooling of the heating surface is one of the most efficient and feasible [8,9]. At the same time, using carbon-based nanofluids in the spray cooling or direct cooling system has been proven to be a highly effective way to enhance heat transfer in the selection of cooling working fluids [10,11]. Therefore, droplet evaporation heat transfer is a critical process in spray cooling, and it becomes crucial to study the evaporation dynamics of carbon-based nanofluids on silicon surfaces.

So far, various studies have identified several factors that can influence the evaporation dynamics of carbon-based nanofluid droplets, like nanoparticle geometries [12], the use of surfactants [13], and surface properties [14]. Similarly, whether at hydrophilic or hydrophobic surfaces, the substrate temperature significantly affects the droplet evaporation dynamics [15]. Al-Sharafi et al. [16] based on the CNT load droplets to observe the internal flow process after heating, and the results show that heating the top and bottom surfaces of the droplet simultaneously results in the formation of four circulating units within the droplet. Chen et al. [17] heated graphene nanofluid droplets on a sapphire substrate and found that despite the high evaporation efficiency of graphene nanofluid droplets at ambient temperatures, the evaporation rate of water was much higher than that of 0.25 mg/ml of rGO-PEG nanofluid when the substrate temperature was higher, which could be attributed to the thermal Marangoni effect. Al-Sharafi et al.

* Corresponding author.
E-mail address: yuying.yan@nottingham.ac.uk (Y. Yan).

https://doi.org/10.1016/j.ijthermalsci.2024.109549
Received 23 August 2024; Received in revised form 18 October 2024; Accepted 12 November 2024
Available online 15 November 2024

[18] based on trichlorooctadecylsilane hydrophobic coating, the carbon nanotube nanofluid droplets were heated at a constant temperature, and the results of the study showed that the Marangoni force and Buoyancy force would combine and form a circulating region in the interior of the droplet. Two counter-rotating circulating regions would be formed in the upper part of the droplet when the contact angle was 110°–150°. Siddiqui et al. [19] conducted droplet evaporation experiments by placing silver and graphene mixed nanofluid droplets on a heated copper surface and showed that the higher the proportion of graphene, the greater the evaporation rate in the range of substrate temperatures from 25 to 100 °C. At the same time, the evaporation residue of nanofluid droplets with pure graphene or a high proportion of graphene can effectively promote the evaporation efficiency of subsequent droplets by up to 370 % [20]. Patil et al. [21] based on polystyrene latex beads loaded with droplets, found that on hydrophilic glass substrates, the height of the deposited ring decreases as the substrate temperature increases, but on treated hydrophobic silicon surfaces, the height of the deposited ring increases as the substrate temperature increases, which have been attributed to the Marangoni effect. Yan et al. [22] based on gold nanofluid droplets, found that the change in droplet volume evaporation was non-linear by heating the glass substrate. Still, droplet volume evaporation became linear when the heating method was changed to external optical plasma heating. At the same time, the addition of carbon-based material could also affect the sessile droplet evaporation mode. Zhong et al. [23] pointed out that the graphite particles can enhance the pinning effect and inhibit the increase of the contact angle and the contraction of the contact line during the evaporation of sessile ethanol droplets, and the graphite nanoparticles loaded droplets can exhibit more substantial pinning effect when compared with pure water droplets. To date, although many studies on carbon-based nanofluid droplets have been carried out, there are not many comparative studies on the evaporation of droplets loaded with multi-walled carbon nanotubes and multilayer graphene, which are typical and widely used carbon-based nanomaterials. In addition, in the context of the enormous application potential of carbon-based nanomaterials in electronic device cooling, comparative studies on their evaporation dynamics on heated silicon wafers are even rarer and need further exploration.

In the process of evaporation of carbon-based nanofluid droplets, the sedimentary of nanoparticles is inevitably accompanied, and the sedimentary process would not only affect the enhanced heat transfer process of the cooling system but also should be considered in the manufacture of electronic equipment [24,25] and inkjet printing [26]. Similarly, the substrate temperature will also have a significant impact on the deposition process. Malla et al. [27] show that the heterogeneous heating of the substrate can alter the sedimentary pattern of nanofluid droplets. Guo et al. [28] pointed out that with the increase of the polyimide substrate temperature, single-walled carbon nanotubes (SWCNTs) deposition achieves higher alignment in the triple line region. As the substrate temperature increases, it becomes more misaligned. Tao et al. [29] studied the evaporation of Al_2O_3 nanofluid droplets on the surface of PTFE. They found that the change in substrate heating temperature can significantly change the deposition mode of the droplets. Liu et al. [30] also based on the Al_2O_3 nanofluid droplets and put them on the heated glass slide. The results show that with the increase of the substrate temperature, the coffee-ring sedimentary pattern becomes more precise, and the inner ring also becomes observable. Lian et al. [31] based on the graphene nanofluid droplet, indicated that when the heating temperature of the substrate increases from 22 °C to 80 °C, the deposition amount inside the deposition ring decreases, which is due to the increase in bottom temperature leading to an increase in evaporation rate and causing the nanoparticles to move towards the contact line area. Liu et al. [32] also studied the evaporation of magnetic nanofluids on Si wafers, and the results showed that the sedimentary pattern would change from a uniform or coffee-ring distribution to a double-ring pattern when the temperature ranged from 10 °C to 70 °C. Wang et al. [33] based on the MWCNT inkjet print process, point out that the instability of inkjet deposition film can be suppressed by increasing the substrate temperature, and there has an optimal bottom temperature that reduces drying flow and optimises the uniformity and electrical properties of the printed film. In addition, other properties of droplet evaporation sedimentary of carbon-based nanofluids have also been described. Machrafi et al. [34] pointed out that with the increase of CNT concentration and the higher number of droplets deposition, the surface resistance of the sample will decrease by up to four orders of magnitude. Gigiberiya et al. [35] placed the binary droplets of MWCNTs and platelets on a glass substrate for evaporation study. They found that three different regions could be divided in the sedimentary area, with two patterns of inner boundary grey-ring and outer boundary coffee-ring, which could be attributed to the dispersion of MWCNTs during evaporation. Lian et al. [36] based on the reduced graphene oxide (RGO) to achieve the print of THz closed-ring resonator through enhancement of the coffee-ring effect, which achieved rapid pinning of the droplet and no gaps between the trinomial line and the solute line. It is also worth mentioning that the deposition of liquid nanofluid droplets after evaporation also affects the subsequent heat transfer process of the liquid. After the deposit is formed, the heat transfer capacity and hydrophilicity are enhanced due to the micro-pores on its surface [3,37]. Meanwhile, most studies on the evaporation and sedimentation of nanoparticle-laden droplets have been based on spherical nanoparticles. In contrast, fewer studies have been based on nanoparticles with high aspect ratios like CNT [38], and even fewer comparative studies on their evaporation processes and deposition patterns. Therefore, exploring the evaporative and sedimentary processes of nanofluid droplets from different carbon-based materials and the influence of substrate temperature on them is significant.

In this paper, based on two mature and widely used carbon-based materials, this paper experimentally studies the effect of substrate temperature on the evaporation process of nanoparticle-loaded droplets using a monocrystalline silicon substrate. At the same time, droplet morphology analyzer, infrared observation and optical measurement are used to explore the special relationship between MLG and MWCNTs carbon-based nanoparticles and contact line movement, liquid-vapour interface temperature distribution and particle sedimentary pattern. The difference in the effects of MLG and MWCNTs nanoparticles on droplet evaporation dynamics and sedimentary patterns is revealed. This study is expected to guide direct spray cooling and inkjet printing of electronic devices based on carbon-based nanofluids.

2. Experimental methods

2.1. Experimental setup

The experimental devices and operation process used in this study are shown in Fig. 1 (a). The microscopic morphology of MLG and MWCNTs nanoparticles used in this paper is shown in Fig. 1 (b). The IR camera (FLIR A655sc, United States) is used to observe the temperature distribution of the liquid-vapour interface of nanofluid droplets. The droplet shape analyzer (Biolin Theta Flex, Sweden) measures the nanofluid droplet contact angle, contact line, and volume changes. Besides, the optical profilometer (KLA Zeta 20, United States) is also used in the study to measure the sedimentary pattern after evaporation. At the same time, a 1-inch diameter monocrystalline silicon wafer was selected as the substrate for placing the nanofluid droplets, and the surface of the silicon wafer was polished. The morphology parameters of the polished surface are shown in Table 1. Meanwhile, the monocrystalline silicon wafer is placed on a temperature-controlled heating panel. In this experiment, the temperature control in this article is achieved through a constant temperature water bath. A tubular heater is placed inside the water tank for heating. The internal sensor converts the water temperature into a resistance value, amplified by an integrated amplifier. It outputs a control signal to control the heating power of the

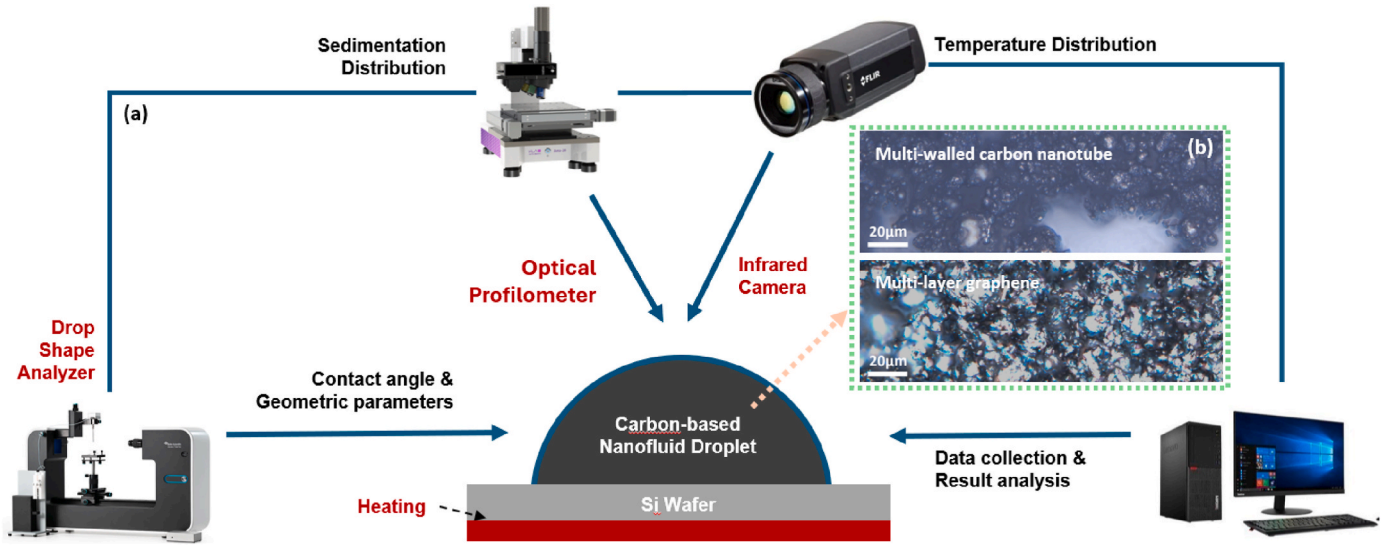

Fig. 1. (a) Experimental setup and operation diagram, and combined (b) microscopic images of MWCNTs and MLG.

Table 1
Silicon wafer polishing surface parameters.

Surface parameters	Value
surface flatness (Total Indicator Reading, TIR)	TIR <3 μm
Warp (Total Thickness Variation, TTV)	TTV <10 μm
Wafer curvature (BOW)	BOW <10 μm
Surface roughness	<0.5 nm
Surface granularity	<10 (for size >0.3 μm)

electric heating tube to keep the water at a constant temperature at 50, 60, 70, and 80 °C, separately. Silicone grease (RS PRO, UK) is used between the silicon wafer and the heating substrate, reducing contact thermal resistance. Before each experiment, each silicon wafer was cleaned by ultrasound in an isopropyl alcohol solution for at least 10 min and then dried using an air jet. And the droplets were extracted and placed using pipettes (Eppendorf Research plus, Germany) during the experiments. The ambient temperature of each test in the laboratory was controlled at 22 ± 2 °C, and the relative humidity was controlled at 55 ± 5 %. At the same time, in this article, the extension of the arithmetic mean height of the line to the surface (*Sa*) is used to describe the distribution and variation of the surface roughness of the sedimentary pattern. The calculation formula of *Sa* is:

$$Sa = \frac{1}{A}\iint_A |Z(x,y)|dxdy \quad (1)$$

2.2. Nanofluid preparation

This study uses multi-walled carbon nanotubes (MWCNTs) and multilayer graphene (MLG) nanoparticles as carbon material, and their physical properties are shown in Table 2. MWCNTs and MLG nanofluid were prepared using the two-step method [39], which can enhance the stability of nanofluids. The nanoparticles and surfactant were then mixed with the solvent using ultrasonic vibration and stirring for at least 30 min, and a nanofluid with good stability was obtained. In this experiment, the deionised water was selected as the base fluid. The nanoparticles were then dispersed into the base liquid. The surfactant sodium dodecyl sulfate (SDS) was also added to the nanofluid, which has been shown to have a significant stabilizing effect on both carbon nanotubes and graphene nanofluids [40,41], and purpose to make the MWCNTs and MLG nanoparticles uniformly and stably dispersed in the liquid and droplet. To conduct a more specific analysis of the sedimentary pattern of nanoparticles, the concentration of nanoparticles was selected as 0.5 wt% in this article. This is because if the mass concentration of nanoparticles is too low or too high, the sedimentary pattern and coffee ring effect will be unclear, which is not conducive to quantitative analysis. There are many studies on the ratio of SDS surfactant concentration and carbon-based nanoparticle concentration. Carbon nanotubes and graphene have different optimal ratios [42,43]. In this article, a mass concentration ratio of nanoparticles to surfactant of 1:2 was selected to minimise the influence of surfactant as much as possible. Therefore, the mass concentration of SDS in this article is 1.0 wt%. It is also worth mentioning that adding surfactants will enhance the thermal conductivity of carbon-based nanofluids [44,45], facilitating droplet evaporation.

Table 2
Basic physical parameters of nanoparticles.

	MWCNTs	MLG
Diameter	Inner: 3–5 nm; Outer: 8–15 nm	7–10 μm
Length/Thickness	3–12 μm	<100 nm (1–3 layers)
Carbon content	>95 wt%	>98 wt%
Density (g/cm^3)	0.15	0.08–0.13
Thermal conductivity (W/m·k)	2000-6000 [46]	2000-6000 [47]

3. Results and discussion

3.1. Effect of different carbon-based nanoparticles on the droplet evaporation dynamics

In this study, the effect of different additions of carbon-based nanoparticles on droplet wetting properties and evaporate modes compared to pure DI water was carried out, and the substrate heating temperature was controlled at 50 °C. As shown in Fig. 2(a–d), compared with pure DI water, adding MWCNTs and MLG nanoparticles can significantly reduce the contact angle and evaporation time of droplets. It is worth mentioning that in the process of contact angle measurement, when the contact angle is lower than 4°, it becomes difficult to observe its change stably, so the changing trend of the contact angle below 4° is described by a dotted line in Fig. 2. At the same time since the evaporation process during this period is very short and accounts for a very small proportion of the total evaporation time, it is not considered in the

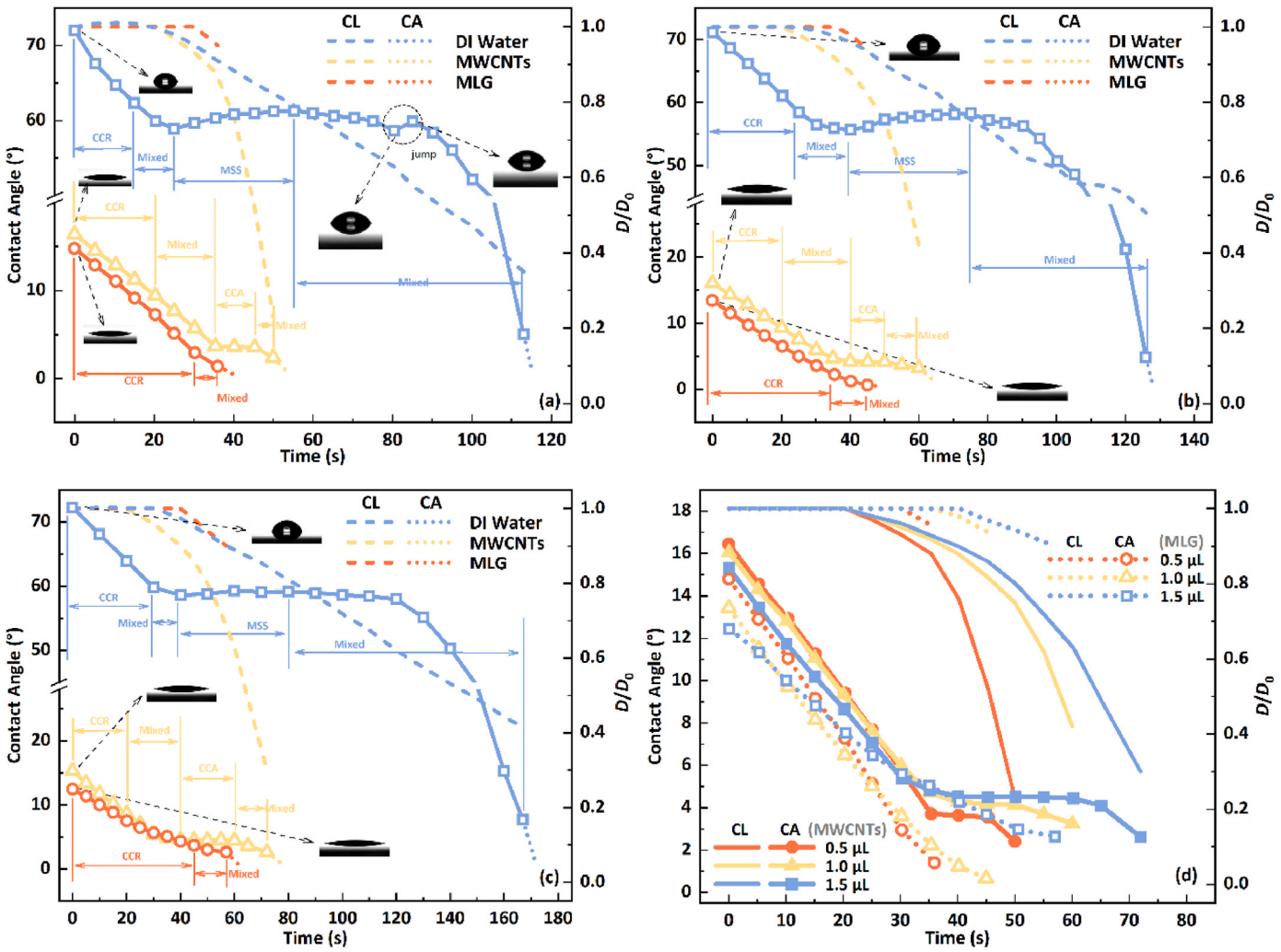

Fig. 2. Changes in contact angle and contact line during evaporation for (a) 0.5 μL, (b) 1.0 μL, (c) 1.5 μL DI water, MWCNTs, and MLG nanofluid droplets and (d) the carbon-based nanoparticles comparison.

calculation of the droplet evaporation life and evaporation rate due to its limited impact. This kind of treatment will also be provided in the subsequent article. From Fig. 2 (a) to Fig. 2 (c), when the droplet volume increases from 0.5 μL to 1.5 μL, the contact angle of the carbon-based nanofluid droplets is all around 15°, while the contact angles of the pure water droplets are all around 72°. At the same time, compared with pure water, adding MWCNTs and MLG nanoparticles can reduce the total evaporation time of droplets by an average of 55 % and 66 %, respectively. This should be due to the addition of carbon-based nanoparticles, which significantly increase the thermal conductivity of the droplets, thus enhancing the heat transfer and evaporation efficiency. At the same time, the addition of nanoparticles also considerably changes the evaporation mode of droplets. As shown in Fig. 2 (a), when pure water droplets evaporate on the Si wafer, it is in the early stage's constant contact radius (CCR) mode. Then, the droplets change to the mixed evaporation mode in which the contact line (CL) and contact angle (CA) decrease simultaneously. As the evaporation proceeds further, the contact line of the droplets continues to decline, but the contact angle increases, which kind of state could be called mixed stick−slip (MSS) mode [48]. Afterwards, the evaporation mode returned to the mixed mode, and the contact angle jumping behaviour appeared in this process. At the same time, when a 0.5 μL MWCNTs nanofluid droplet evaporates on the Si wafer, the droplet is also in the CCR mode in the initial stage, then transitions to the mixed mode and CCA mode and ends in the mixed mode in the final stage of evaporation. Meanwhile, when 0.5 μL MLG nanofluid droplets evaporate on the Si wafer, the droplet evaporation remains in the CCR mode and changes to the mixed mode in the final stage. Also shown in Fig. 2 (b) and (c), when the droplet volume increases to 1.0 and 1.5 μL, the evaporation modes experienced by the three droplets remain unchanged. Among them, the CCR mode takes the longest time during the evaporation process of MLG nanofluid droplets, and it may be attributed to the addition of MLG nanoparticles and surfactant that reduces the surface tension, making it insufficient to drive the movement of the contact line. In addition, as shown in Fig. 2 (d), compared with MWCNTs, the addition of MLG can always lead to better wettability of droplets and higher evaporation efficiency, which can be mainly attributed to the enhancement of thermal conductivity and wettability.

Subsequently, under the same external conditions, during the evaporation process of different types of droplets, the temperature difference (T_{diff}) between the top of the droplet and the contact line region changes with time, as shown in Fig. 3(a–d). The T_{diff} is the difference between the droplet liquid-vapour interface vertex temperature T_2 and the contact line region temperature T_1. As shown in Fig. 3 (a), when the droplet volume is controlled to 0.5 μL, the T_{diff} of the DI water droplets is significantly higher than that of MWCNTs and MLG nanofluid droplets. For example, in the initial stage, the T_{diff} of DI water droplets is about 3.7 °C, while the T_{diff} of MWCNTs and MLG nanofluid droplets are about 0.9 and 0.5 °C, respectively. This may be attributed to the enhanced liquid thermal conductivity and wettability suppressing the evaporative

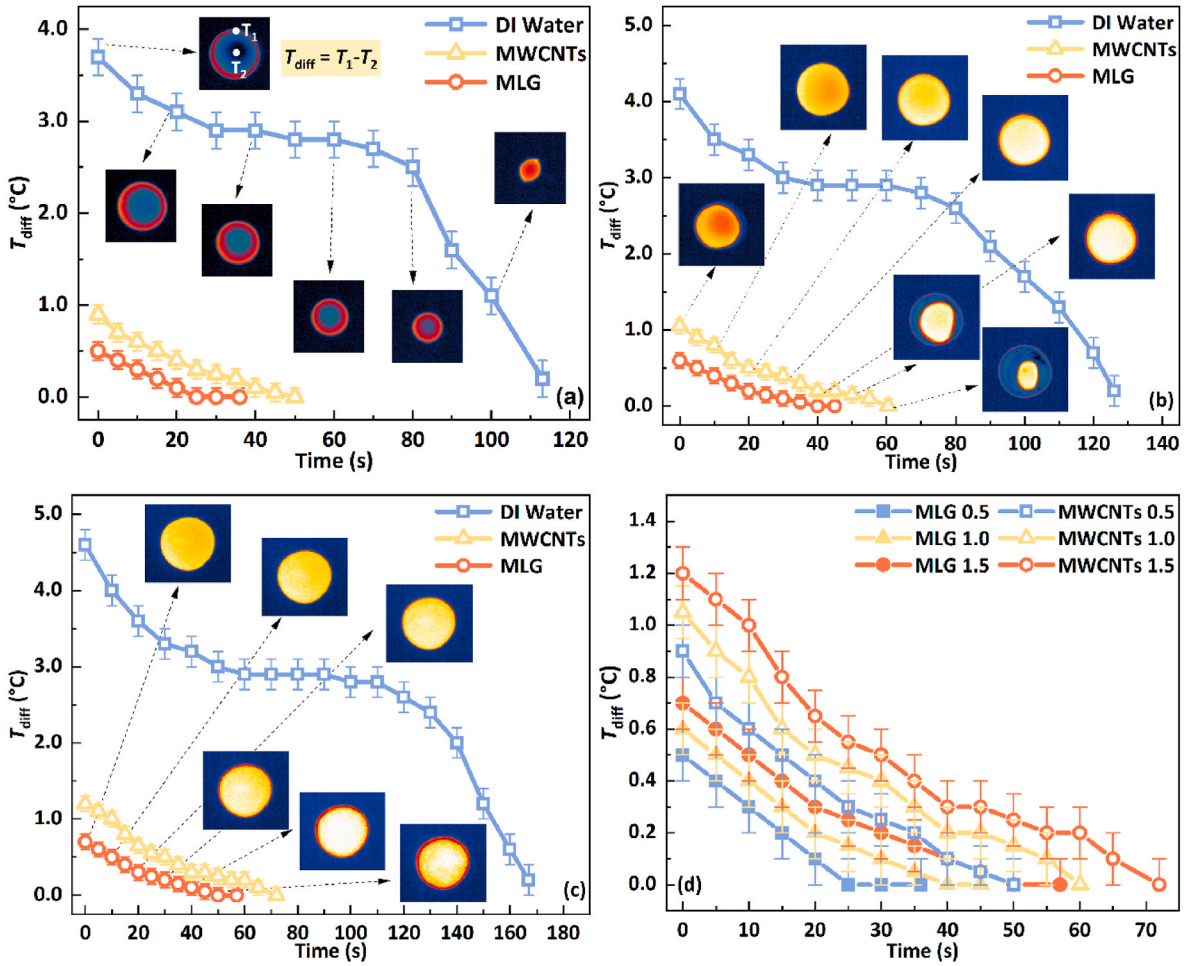

Fig. 3. Temperature difference at the edge and top of liquid-vapour interface of (a) 0.5 μL, (b) 1.0 μL, (c) 1.5 μL DI water, MWCNTs, and MLG nanofluids with time.

cooling effect. At the same time, it is also evident from the illustration in Fig. 3 (a) that as the evaporation process proceeds, the temperature uniformity of the droplet liquid-vapour interface is improved, and the evaporative cooling effect is also suppressed. Similarly, when the droplet volume increases to 1.0 μL and 1.5 μL, the T_{diff} of the droplet changes with time, as shown in Fig. 3 (b) and (c). As the droplet volume increases, the T_{diff} also increases at the initial moment, such as the T_{diff} of DI water droplet increased by 11 % and 24 % when the volume rises to 1.0 μL and 1.5 μL, respectively. In addition, the changes of T_{diff} with time for MWCNTs and MLG nanofluid droplets under different volume conditions are shown in Fig. 3 (d). Compared with MLG nanofluid, the T_{diff} of MWCNTs nanofluid droplets is always larger. For example, under the conditions of 0.5 μL, 1.0 μL, and 1.5 μL, the T_{diff} increases by 80 %, 75 %, and 71 %, respectively. It may be owed that the addition of MLG nanoparticles makes the surface tension of the liquid more minor, and the droplet wettability is more muscular, which strengthens the thermal conductivity inside the droplet, thereby inhibiting the evaporative cooling effect.

At the same time, the dimensionless volumes (V/V_0) of different volumes change with time during the evaporation process, where V refers to the real-time volume of the droplet, and V_0 refers to the initial volume of the droplet. It can be seen from Fig. 4 (a) that when the droplet volume is 0.5 μL, the average evaporation rate of the carbon-based nanofluid droplets is greater, and compared with pure DI water, the addition of MWCNTs and MLG nanoparticles makes the average evaporation rate of the droplets increased by approximately 1.2 and 2.1 times, respectively. It is worth mentioning that, for the convenience of analysis, as mentioned above, the change in volume at the final stage of droplet evaporation (contact angle less than 4°) is ignored and the evaporation is assumed to be complete. Similarly, as shown in Fig. 4 (b), when the droplet volume is 1.0 μL, adding MWCNTs and MLG nanoparticles increases the average evaporation rate of the droplets by approximately 1.2 and 1.9 times compared with pure DI water droplets. When the droplet volume increased to 1.5 μL, this value became 1.36 and 2 times. At the same time, the comparison of different carbon-based nanofluid droplet average evaporation rates at different volumes is shown in Fig. 4 (d). It can be seen from Fig. 4 (d) that the evaporation rate of the MLG nanofluid droplets is still faster than MWCNTs nanofluid droplets. At the same time, with the increase of the droplet volume, the evaporation rate of the droplets loaded with carbon-based nanoparticles increases faster than that of the DI water droplets, which can be attributed to the fact that the evaporative cooling effect at the liquid-vapour interface is more obvious on the DI water droplets, thereby inhibiting evaporation more severely.

3.2. *Effect of substrate temperature on the droplet evaporation dynamics*

After exploring the effects of different materials, this study is also conducted on the effects of different substrate temperatures on the droplet evaporation process. As shown in Fig. 5, different droplets exhibit different evaporation processes at various temperatures. As the substrate temperature increases, the total evaporation time shortens significantly. The effect of substrate temperature on the evaporation of the DI water droplets is shown in Fig. 5 (a). When the temperature increases from 60 °C to 80 °C, the total evaporation time is shortened by approximately 63 %. Under different substrate temperature conditions,

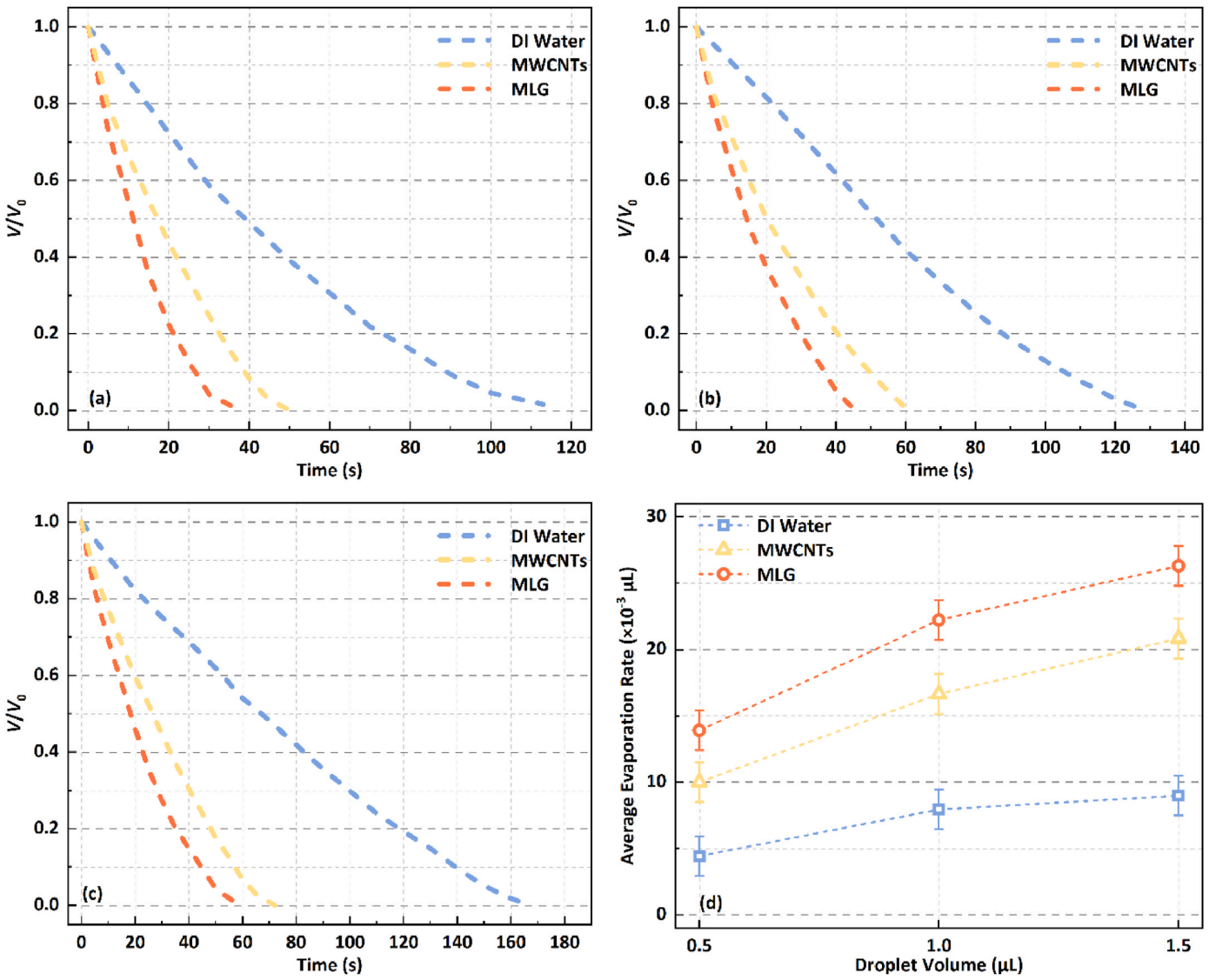

Fig. 4. (a) 0.5 μL, (b) 1.0 μL, (c) 1.5 μL droplet dimensionless volume changes with time of DI water and carbon-based nanofluid, (d) the average evaporation rate of DI water and carbon-based nanofluid droplet with different volume.

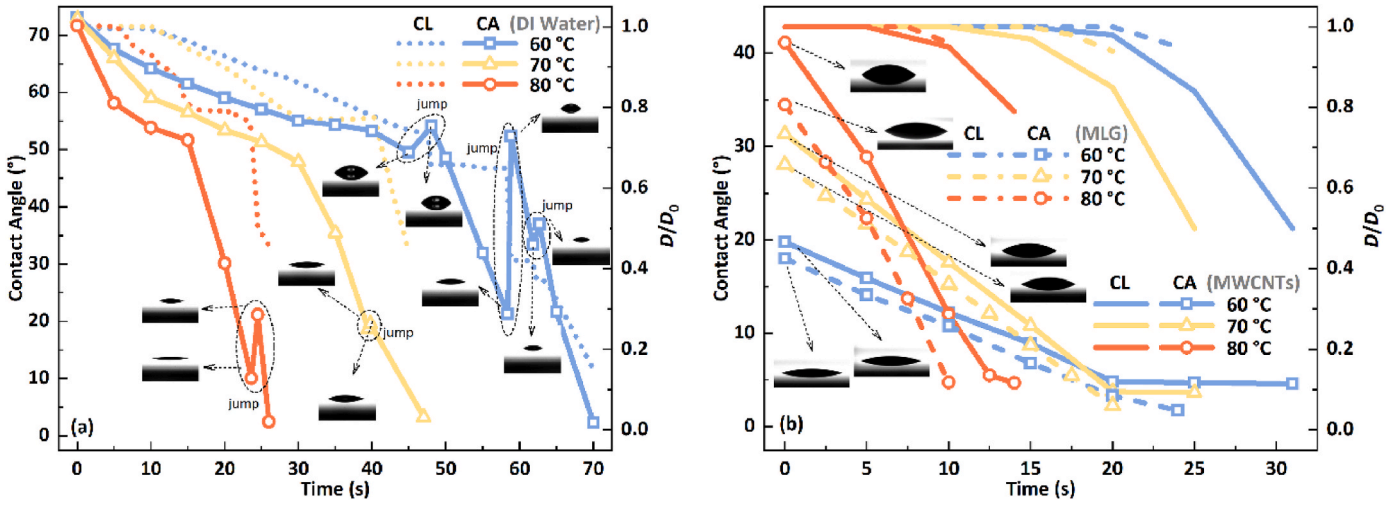

Fig. 5. Changes in contact angle and contact line of 0.5 μL (a) DI water and (b) carbon-based nanoparticle-laden droplets during evaporation.

the contact line will appear jumping phenomenon during the droplet evaporation. For example, when the substrate temperature is 60 °C, around the 58th second of the evaporation process of DI water droplets, the contact angle immediately increases from 21° to 52° after jumping, and the contact line is also instantly reduced by about 34 %. At the same time, as shown in Fig. 5 (b), as the substrate temperature increases, the total evaporation time of the carbon-based nanofluid droplets also significantly decreases. When the substrate temperature increases from 60 °C to 80 °C, the total evaporation time of MWCNTs and MLG nanofluid droplets decreases by about 54 %. Meanwhile, the initial contact angle also increases significantly with substrate temperature. When the substrate temperature increases from 60 °C to 80 °C, the contact angles of MWCNTs and MLG nanofluid droplets increase by about 1.1 times and 0.9 times, respectively. As the temperature increases, the evaporation process of the MLG nanofluid droplets only experiences the CCR mode and the mixed mode. Still, the MWCNTs nanofluid droplet base has CCR, CCA, and mixed evaporation modes during the entire evaporation process.

Under the same conditions, when the volume of the droplets increases to 1.0 μL, the evaporation process of DI water, MWCNTs, and MLG nanofluid droplets is shown in Fig. 6. With the volume increased to 1.0 μL, the DI water droplets still showed apparent jumping behaviour at the substrate temperature of 70 °C and 80 °C. At the same time, the entire evaporation process was relatively smooth at the substrate temperature of 60 °C. For 1.0 μL MWCNTs and MLG nanofluid droplets, the increase in substrate temperature significantly shortened the total evaporation time. At various temperatures, the increase in droplet volume did not affect the evaporation modes of MWCNTs and MLG nanofluid droplets. Meanwhile, when the droplet volume increases to 1.5 μL, the evaporation process changes with time, as shown in Fig. 7. As shown in Fig. 7 (a), the 1.5 μL DI water droplet contact line only jumped at 80 °C. The droplet contact angle increased instantly from 30° to 56° at about 25th seconds. Likewise, as shown in Fig. 7 (b), the evaporation mode of MWCNTs and MLG nanofluid droplets also do not change with increasing droplet volume and are the same as those at 0.5 μL and 1.0 μL.

As the substrate heating temperature increases, as shown in Fig. 8 (a–i), the maximum value of the temperature difference ($T_{diff,\ max}$) at the top and edge of the droplet's liquid-vapour interface also changes. The $T_{diff,\ max}$ of DI water droplets with different volumes would be changed with the substrate temperature, as shown in Fig. 8(a–c). When the droplet volume increases from 0.5 μL to 1.5 μL, $T_{diff,\ max}$ will also rise as the substrate temperature increases. This may be due to the increased evaporation rate at the liquid-vapour interface. This causes the surface to absorb much heat, promoting the evaporation-cooling effect. In addition, as the droplet volume increases, the $T_{diff,\ max}$ will also increase. For example, when the substrate temperature is 80 °C, the $T_{diff,\ max}$ will increase by about 17 % from 0.5 μL to 1.5 μL. This is because, with the increase in droplet volume, the distance between the liquid-vapour interface and the substrate also increases, inhibiting heat transfer and making a more significant temperature difference between the top and edge of the interface. Similarly, the changes in $T_{diff,\ max}$ of MWCNTs and MLG nanofluid droplets under different volumes and substrate temperatures are shown in Fig. 8(d–f) and (g-i), respectively. It can be seen that the $T_{diff,\ max}$ of carbon-based nanofluid droplets, is still lower than that of DI water. For example, when the substrate temperature is 80 °C and volume is 0.5 μL, the $T_{diff,\ max}$ of MWCNTs, and MLG nanofluid droplet are 37 % and 45 % lower than DI water, respectively. This is due to the addition of carbon-based nanoparticles significantly enhancing the droplets' wettability and internal heat transfer ability, which can effectively suppress the evaporative cooling effect of the liquid-vapour interface and improve its temperature uniformity. Compared with DI water and MWCNTs nanoparticles, adding MLG nanoparticles could make $T_{diff,\ max}$ with a max reduction of up to 3.7 °C and 1.0 °C, respectively. It means that the addition of MLG nanoparticles will make the effect of inhibiting evaporative cooling more apparent, which can be attributed to MLG nanofluid droplets having better wettability.

At the same time, the change in substrate temperature on the dimensionless volume (V/V_0) of the DI water and carbon-based nanofluid droplets is shown in Fig. 9(a–d). It can be seen from Fig. 9 (a) that as the droplet volume is 0.5 μL, the substrate temperature would significantly affect the change of the V/V_0. With the increase in the substrate temperature, the slope of the curve gradually increases, which means that the droplet's evaporation rate also gradually increases. Similarly, when the droplet volume increases to 1.0 μL and 1.5 μL, the changing trend of V/V_0 of the droplets remains consistent, and the effect of temperature on V/V_0 is still pronounced. Moreover, the slope of the V/V_0 curve of the droplets loaded with MLG and MWCNTs is always greater than that of the DI water, indicating that adding carbon-based nanoparticles can significantly enhance evaporation. Meanwhile, under the combined effect of droplet volume and substrate temperature, the overall average evaporation rate change is shown in Fig. 9 (d). It can be seen that when the base temperature is 60 °C, 70 °C and 80 °C, the evaporation rate of the MLG-loaded droplets can be increased by up to 1.9, 1.3 and 1.2 times compared with DI water. Besides, the average evaporation rate of MLG nanofluid droplets is always higher than that of MWCNTs nanofluid droplets. As shown in Fig. 9 (d), when the droplet volume is 0.5 μL, the average evaporation rate of MLG nanofluid droplets is 27 % higher. When the droplet volume increases to 1.0 and 1.5 μL, this value becomes 20 % and 25 %, respectively.

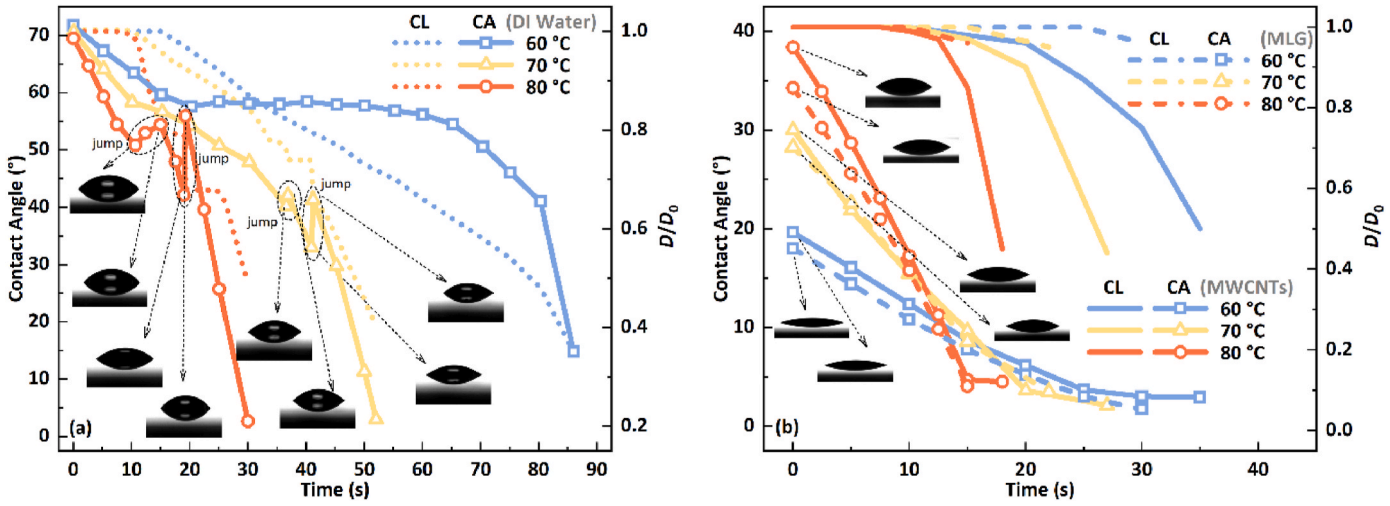

Fig. 6. Changes in contact angle and contact line of 1.0 μL (a) DI water and (b) carbon-based nanoparticle-laden droplets during evaporation.

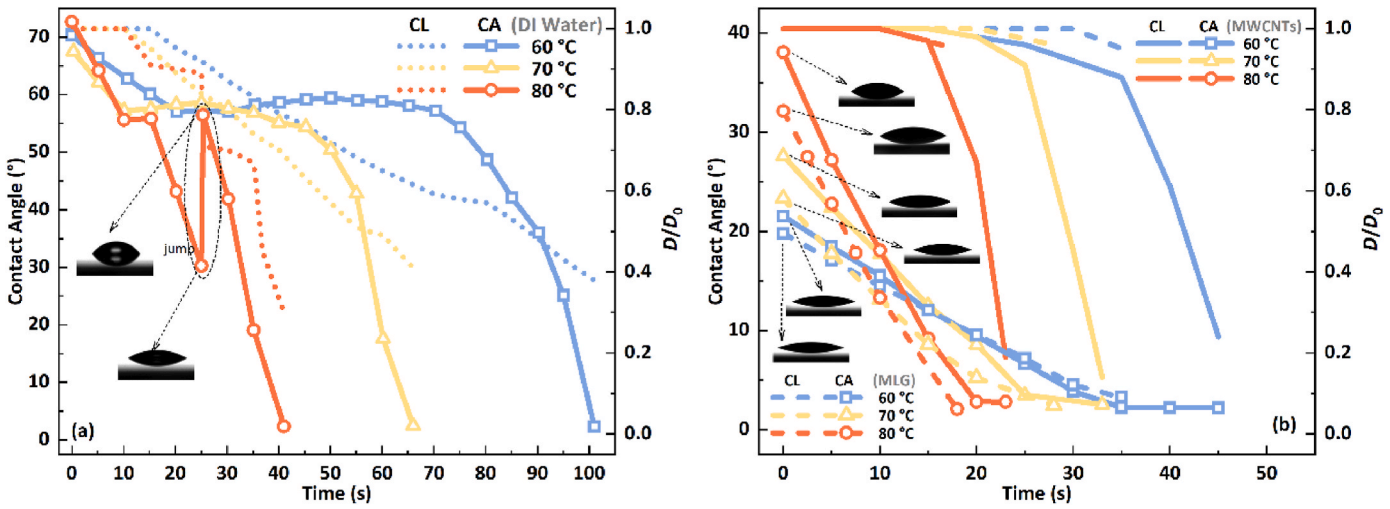

Fig. 7. Changes in contact angle and contact line of 1.5 μL (a) DI water and (b) carbon-based nanoparticle-laden droplets during evaporation.

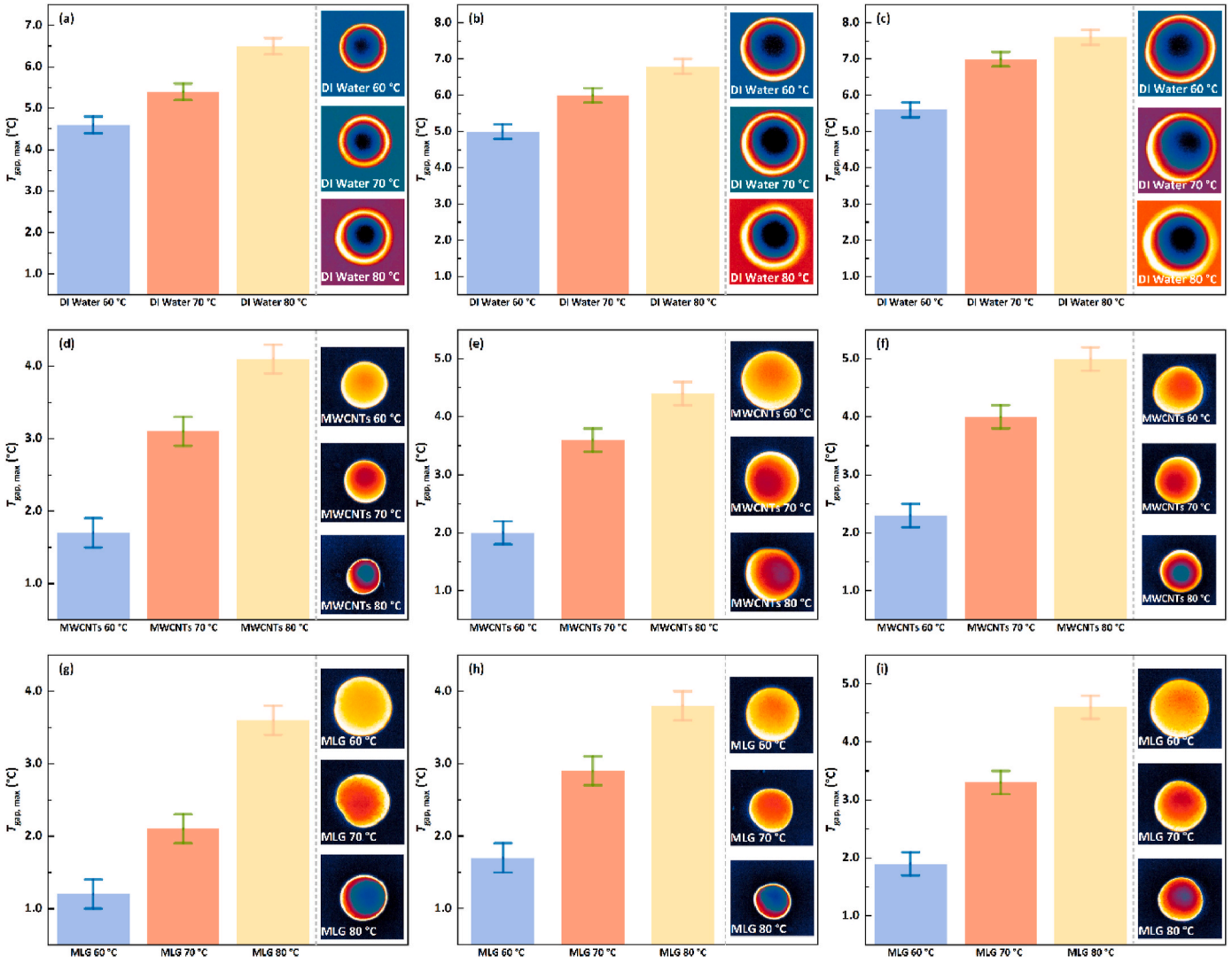

Fig. 8. Based on different substrate temperatures, the maximum temperature difference between the top and edge of (a) 0.5 μL, (b) 1.0 μL, (c) 1.5 μL DI water droplet, (d) 0.5 μL, (e) 1.0 μL, (f) 1.5 μL MWCNTs nanofluid droplet, and (g) 0.5 μL, (h) 1.0 μL, (i) 1.5 μL MLG nanofluid droplet.

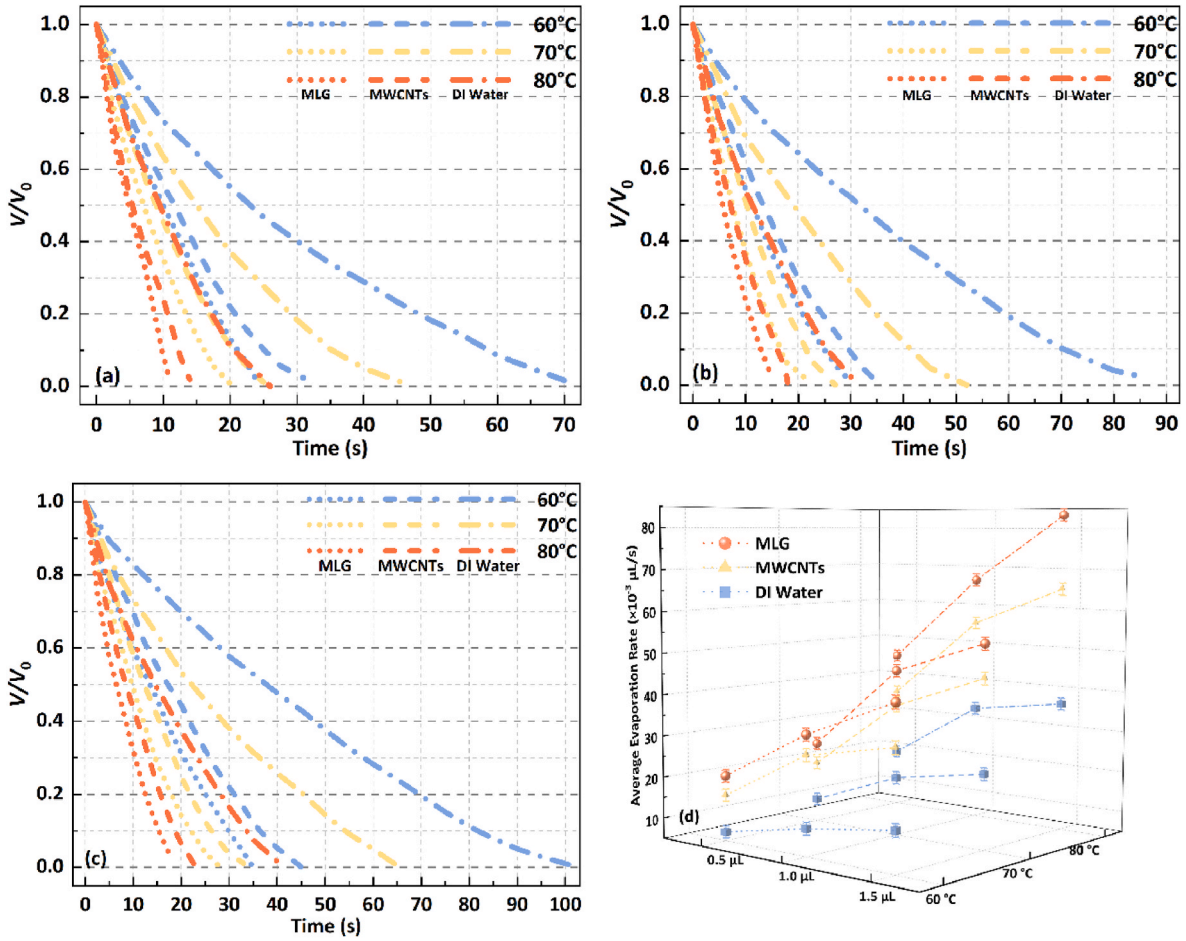

Fig. 9. Dimensionless volume changes under different substrate temperatures of (a) 0.5 μL, (b) 1.0 μL (c) 1.5 μL DI water and carbon-based nanofluid droplets, (d) the average evaporation rate of DI water and carbon-based nanofluid droplets with different volume and temperature conditions.

3.3. Macroscopic effects of carbon-based materials on the sedimentary pattern

After evaporation, the carbon-based nanoparticles loaded in the droplets will be deposited on the silicon wafer's surface, creating a coffee-ring effect. The sedimentary patterns formed after evaporation of carbon-based nanofluid droplets of different volumes when the substrate temperature (T_{sub}) is 50 °C are shown in Fig. 10. It can be seen from Fig. 10(a–c) that as the droplet volume increases, the area of the sedimentary pattern formed after the MLG nanofluid droplets evaporate also increases, and the deposition pattern has an apparent coffee-ring effect. This is because MLG nanofluid droplets mainly follow the CCR evaporation mode during evaporation, so MLG nanoparticles will always accumulate in the contact line area through the Marangoni flows inside the droplet during the evaporation process, which will lead to a noticeable coffee-ring effect. At the same time, it can be seen from Fig. 10(d–f) that the area of the sedimentary pattern formed after the MWCNTs nanofluid droplets evaporate also increases with the increase in droplet volume. However, compared with MLG nanofluid, the coffee ring effect of the deposited pattern is weaker. This phenomenon is because the droplets of MWCNTs nanofluids mainly follow the CCA and Mixed modes during evaporation, making the contact line shrink inward. In addition, the effect of different nanoparticles on the surface roughness *Sa* is also shown in Fig. 11. At the same time, regions 1 and 2 are located inside the sedimentary pattern, region 3 near the coffee ring, and region 4 outside the sedimentary pattern. The comparison between Fig. 11 (a) and (b) shows that the deposition of MLG particles leads to a rougher sedimentary pattern, which is caused by the uneven deposition distribution inside the coffee ring. At the same time, it can be seen from Fig. 11 (a) that in the deposition of MLG nanoparticles, the roughness decreases as it approaches the outside, and the surface roughness of region 3 decreases by an average of 28 % compared with regions 1 and 2. Besides, Fig. 11 (b) shows that in the deposition of MWCNT nanoparticles, the roughness in region 2 of the sedimentary pattern is the lowest, and an average of 32 % reduces its surface roughness compared with regions 1 and 3.

In addition, when the substrate temperature is increased from 60 to 80 °C, the sedimentary patterns with different volumes are shown in Fig. 12. The sedimentary pattern of MLG nanofluid droplets still shows a more apparent coffee-ring effect with the increase in substrate temperature. From the comparison of Fig. 12 (a), (c), and (e), the substrate temperature has no noticeable effect on the sedimentary pattern of MLG nanofluid droplets. However, with the increase in droplet volume, the number of nanoparticles deposited in the central region increases. This may be because as the volume increases, the number of loaded nanoparticles and the total evaporation time also increases, and they will be deposited in the central area based on gravity during the evaporation process. This can be attributed to the fact that as the volume increases, the number of loaded nanoparticles also increases and will be deposited in the central region based on gravity during evaporation. At the same time, from the comparison in Fig. 12 (b), (d), and (f), the volume change has no noticeable effect on the sedimentary pattern of MWCNTs nanofluid droplets. Still, the change in the substrate temperature will have little impact on the sedimentary pattern. The deposition of MWCNTs nanoparticles in the central area becomes lighter when the substrate temperature increases from 60 to 80 °C. This is because as the

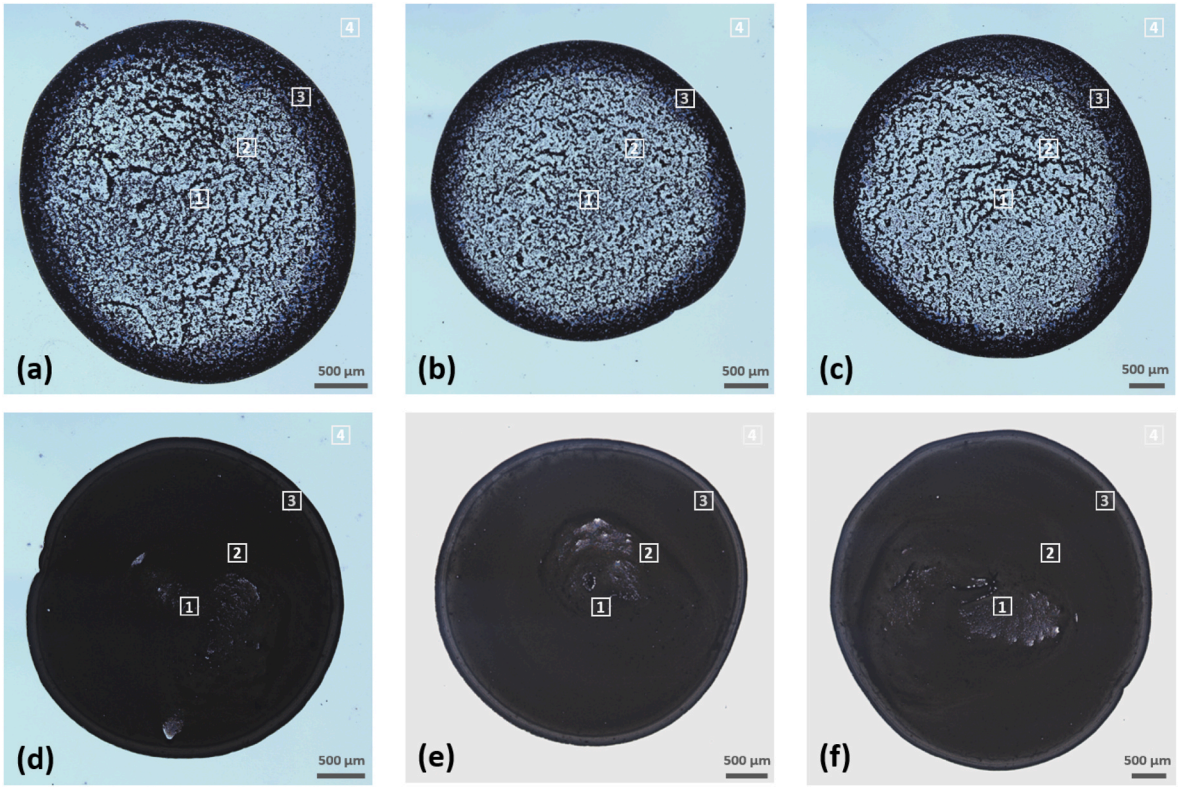

Fig. 10. When the substrate temperature is 50 °C, the sedimentary pattern of (a) 0.5 μL, (b) 1.0 μL, (c) 1.5 μL MLG nanofluid droplets, and (d) 0.5 μL, (e) 1.0 μL; (f) 1.5 μL MWCNTs nanofluid droplets, and regions 1, 2, 3 and 4 in the figure are the areas for calculating surface roughness.

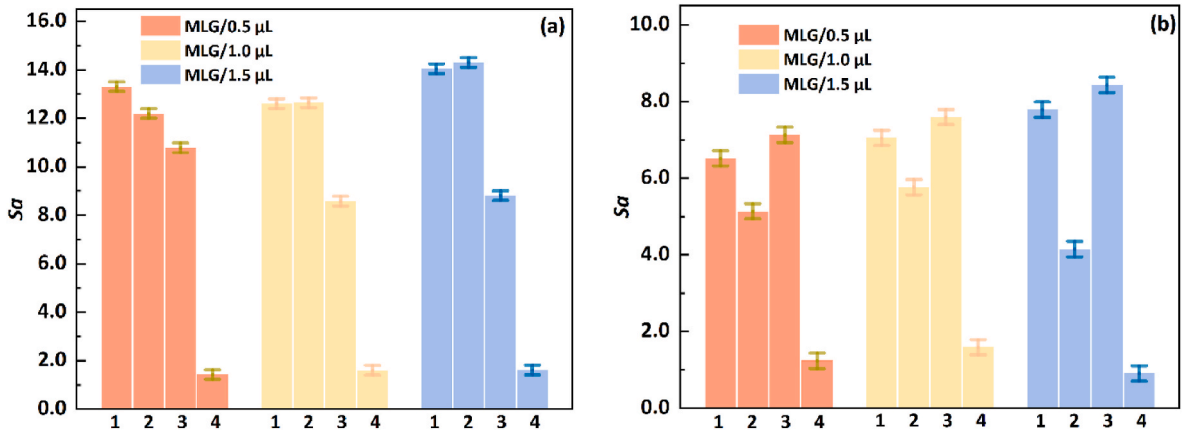

Fig. 11. Effect of the deposition distribution of (a) MWCNTs nanoparticles and (b) MLG nanoparticles on the surface roughness of regions 1–4 under different volume conditions.

temperature increases, the duration of the CCA mode becomes shorter, and more nanoparticles accumulate toward the contact line area, which results in less deposition in the central area. In addition, Fig. 13(a–c) shows the effect of temperature change on the roughness of the sedimentary pattern. It can be seen that when the temperature increases, the average surface roughness in the MWCNTs sedimentary pattern increases slightly. From 60 to 80 °C in each volume, the average increase in the *Sa* is about 25 %. This phenomenon is caused by the uneven distribution of internal particle deposition caused by the rise in substrate temperature. At the same time, when the temperature increases, the average surface roughness of the MLG sedimentary pattern fluctuates, and the average fluctuation range is about 16 % from 60 to 80 °C in each volume. This shows that the temperature change has little effect on the roughness distribution of the sedimentary pattern of the MLG droplet. In addition, it can be seen that no matter what the conditions are, the average surface roughness of the non-deposition area always fluctuates between 1.0 and 2.0, and the deposition of MLG particles always causes a greater surface roughness, which increases by about 1.8 times compared with MWCNTs.

4. Conclusion

This article compared the effects of two kinds of typical carbon-based nanomaterials, MLG and MWCNTs on droplet evaporation dynamics. At the same time, monocrystal silicon is selected as the substrate, and the substrate heating is controlled between 50 °C and 80 °C to better fit the thermal management situation of high heat flux electronic devices such as chips. These results show that adding carbon-based nanoparticles can

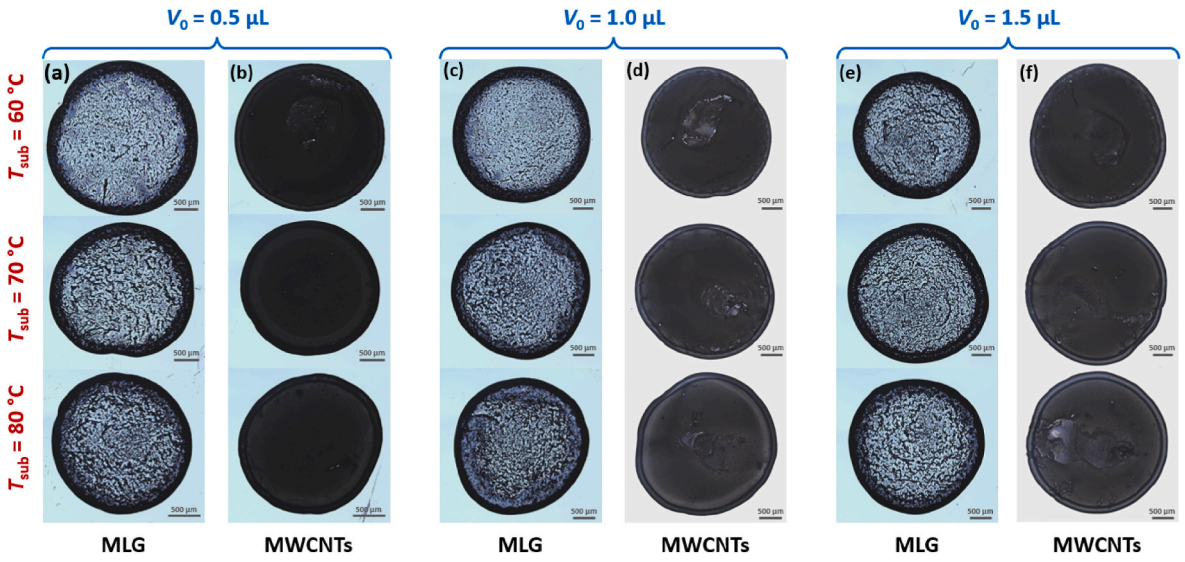

Fig. 12. Under different volume conditions, the sedimentary patterns of MLG nanofluid droplets when the substrate temperature is (a) 60 °C, (c) 70 °C, (e) 80 °C, and the sedimentary patterns of MWCNTs nanofluid droplets when the substrate temperature is (b) 60 °C, (d) 70 °C, (f) 80 °C.

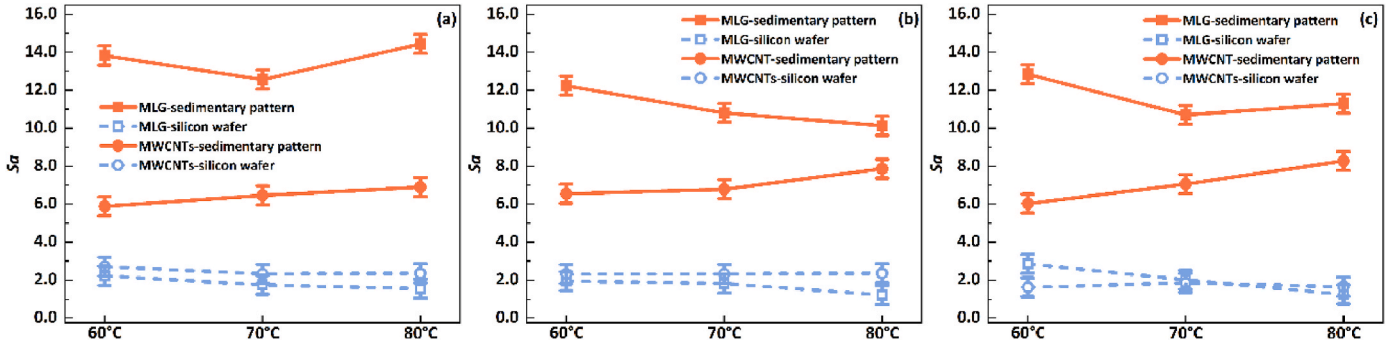

Fig. 13. Variation trend of average surface roughness inside and outside the coffee ring in the deposition pattern of (a) 0.5 μL, (b) 1.0 μL, (c) 1.5 μL droplets under different substrate temperature conditions.

significantly improve evaporation efficiency by up to 2.1 times compared with pure DI water, effectively enhancing the heat transfer process. At the same time, droplets loaded with MLG nanoparticles have the fastest evaporation efficiency, owing to the MLG nanoparticles can make the droplets better wettability. At the same time, with the increase of substrate temperature, MLG nanofluid droplets always have a better heat transfer effect. As the substrate temperature increases, the initial contact angle of the carbon-based nanofluid droplets also increases, while that of the DI water droplets decreases slightly. At the same time, the change in substrate temperature has no noticeable effect on the evaporation mode of carbon-based nanofluid droplets. Still, the simultaneous change of droplet volume and substrate temperature significantly affects the jumping behaviour of the DI water droplets. Furthermore, based on various substrate temperatures and droplet volumes, MLG nanoparticles consistently have the best effect of suppressing the evaporative cooling phenomenon, reducing the initial $T_{diff,\ max}$ by up to 3.7 °C compared to DI water. In addition, after evaporation, the MLG and MWCNTs nanoparticles also had different effects on the sedimentary pattern. The sedimentary pattern of MLG nanofluid droplets showed a noticeable coffee-ring effect, while loaded MWCNTs nanoparticles inhibited the coffee-ring effect. In addition, MLG nanoparticles consistently resulted in greater surface roughness in the sedimentary patterns, which increased by about 1.8 times compared to MWCNTs under various conditions, which can be attributed to the uneven deposition distribution of MLG nanoparticles. This research will guide industrial applications such as spray cooling and inkjet printing based on carbon-based nanofluids.

CRediT authorship contribution statement

Zhihao Zhang: Writing – review & editing, Writing – original draft, Visualization, Validation, Methodology, Investigation, Formal analysis, Data curation, Conceptualization. **Yuying Yan:** Writing – review & editing, Supervision, Resources, Methodology, Funding acquisition, Conceptualization.

Declaration of Competing Interest

The authors declare that they have no known competing financial interests or personal relationships that could have appeared to influence the work reported in this paper.

Acknowledgements

This work was supported by H2020-MSCA-RISE-778104–ThermaSMART, Royal Society (UK) (IEC\NSFC\211210) and doctoral degree scholarship of China Scholarship Council (CSC).

Data availability

No data was used for the research described in the article.

References

[1] N. Jain, E. Gupta, N.J. Kanu, Plethora of Carbon nanotubes applications in various fields–A state-of-the-art-review, Smart Science 10 (2022) 1–24.
[2] A. Razaq, F. Bibi, X. Zheng, R. Papadakis, S.H.M. Jafri, H. Li, Review on graphene-, graphene oxide-, reduced graphene oxide-based flexible composites: from fabrication to applications, Materials 15 (2022) 1012.
[3] M. Asim, F.R. Siddiqui, Hybrid nanofluids—next-generation fluids for spray-cooling-based thermal management of high-heat-flux devices, Nanomaterials 12 (2022) 507.
[4] A.A. Mehrizi, H. Karimi-maleh, M. Naddafi, O. Karaman, F. Karimi, C. Karaman, C. K. Cheng, Evaporation characteristics of nanofuel droplets: a review, Fuel 319 (2022) 123731.
[5] Y. Shang, X. Xiang, Q. Ye, Q. Wu, J. Zhang, J.-M. Lin, Advances in nanomaterial-based microfluidic platforms for on-site detection of foodborne bacteria, TrAC, Trends Anal. Chem. 147 (2022) 116509.
[6] J. Wu, H. Lin, D.J. Moss, K.P. Loh, B. Jia, Graphene oxide for photonics, electronics and optoelectronics, Nat. Rev. Chem 7 (2023) 162–183.
[7] Z. Zhang, X. Wang, Y. Yan, A review of the state-of-the-art in electronic cooling, e-Prime-Advances in Electrical Engineering, Electron. Electric 1 (2021) 100009.
[8] A. Cotler, E. Brown, V. Dhir, M. Shaw, Chip-level spray cooling of an LD-MOSFET RF power amplifier, IEEE Trans. Compon. Packag. Technol. 27 (2004) 411–416.
[9] S.G. Kandlikar, A.V. Bapat, Evaluation of jet impingement, spray and microchannel chip cooling options for high heat flux removal, Heat Tran. Eng. 28 (2007) 911–923.
[10] N. Ali, A.M. Bahman, N.F. Aljuwayhel, S.A. Ebrahim, S. Mukherjee, A. Alsayegh, Carbon-based nanofluids and their advances towards heat transfer applications—a review, Nanomaterials 11 (2021) 1628.
[11] Y.T. Aksoy, Y. Zhu, P. Eneren, E. Koos, M.R. Vetrano, The impact of nanofluids on droplet/spray cooling of a heated surface: a critical review, Energies 14 (2020) 80.
[12] A. Askounis, K. Sefiane, V. Koutsos, M.E. Shanahan, Effect of particle geometry on triple line motion of nano-fluid drops and deposit nano-structuring, Adv. Colloid Interface Sci. 222 (2015) 44–57.
[13] H.Y. Erbil, Control of stain geometry by drop evaporation of surfactant containing dispersions, Adv. Colloid Interface Sci. 222 (2015) 275–290.
[14] A. Al-Sharafi, B.S. Yilbas, A.Z. Sahin, H. Al-Qahtani, Heating analysis of a droplet on stretchable hydrophilic surface, Int. J. Heat Fluid Flow 85 (2020) 108659.
[15] B. Sobac, D. Brutin, Thermal effects of the substrate on water droplet evaporation, Phys. Rev. 86 (2012) 021602.
[16] A. Al-Sharafi, B.S. Yilbas, Thermal and flow analysis of a droplet heating by multi-walls, Int. J. Therm. Sci. 138 (2019) 247–262.
[17] P. Chen, S. Harmand, S. Szunerits, R. Boukherroub, Evaporation behavior of PEGylated graphene oxide nanofluid droplets on heated substrate, Int. J. Therm. Sci. 135 (2019) 445–458.
[18] A. Al-Sharafi, H. Ali, B.S. Yilbas, A.Z. Sahin, M. Khaled, N. Al-Aqeeli, F. Al-Sulaiman, Influence of thermalcapillary and buoyant forces on flow characteristics in a droplet on hydrophobic surface, Int. J. Therm. Sci. 102 (2016) 239–253.
[19] F.R. Siddiqui, C.Y. Tso, S.C. Fu, H. Qiu, C.Y. Chao, Droplet evaporation and boiling for different mixing ratios of the silver-graphene hybrid nanofluid over heated surfaces, Int. J. Heat Mass Tran. 180 (2021) 121786.
[20] F.R. Siddiqui, C.Y. Tso, S.C. Fu, H. Qiu, C.Y. Chao, Evaporation and wetting behavior of silver-graphene hybrid nanofluid droplet on its porous residue surface for various mixing ratios, Int. J. Heat Mass Tran. 153 (2020) 119618.
[21] N.D. Patil, P.G. Bange, R. Bhardwaj, A. Sharma, Effects of substrate heating and wettability on evaporation dynamics and deposition patterns for a sessile water droplet containing colloidal particles, Langmuir 32 (2016) 11958–11972.
[22] X. Yan, J. Xu, Z. Meng, J. Xie, A comprehensive comparison between substrate heating and light heating induced nanofluid droplet evaporations, Appl. Therm. Eng. 175 (2020) 115389.
[23] X. Zhong, F. Duan, Evaporation of sessile droplets affected by graphite nanoparticles and binary base fluids, J. Phys. Chem. B 118 (2014) 13636–13645.
[24] H.W. Tan, Y.Y.C. Choong, C.N. Kuo, H.Y. Low, C.K. Chua, 3D printed electronics: processes, materials and future trends, Prog. Mater. Sci. 127 (2022) 100945.
[25] W. Li, C. Zhang, D. Lan, W. Ji, Y. Wang, Solution printing of electronics and sensors: applicability and application in space, Adv. Eng. Mater. 24 (2022) 2200173.
[26] H. Abdolmaleki, P. Kidmose, S. Agarwala, Droplet-based techniques for printing of functional inks for flexible physical sensors, Adv. Mater. 33 (2021) 2006792.
[27] L.K. Malla, R. Bhardwaj, A. Neild, Colloidal deposit of an evaporating sessile droplet on a non-uniformly heated substrate, Colloids Surf. A Physicochem. Eng. Asp. 584 (2020) 124009.
[28] G.L. Goh, N. Saengchairat, S. Agarwala, W.Y. Yeong, T. Tran, Sessile droplets containing carbon nanotubes: a study of evaporation dynamics and CNT alignment for printed electronics, Nanoscale 11 (2019) 10603–10614.
[29] Y.-Q. Tao, Q.-S. Liu, Conditions of enhanced evaporation for nanofluids droplet and inhibition of coffee-ring effect under buoyancy and Marangoni convection, Surface. Interfac. 42 (2023) 103320.
[30] B. Liu, S. Wang, L. Chai, G. El Achkar, A. Chen, P.E. Theodorakis, Experimental investigation of nanoparticles distribution mechanisms and deposition patterns during nanofluid droplet evaporation, the European Physical, J. Appl. Phys. 92 (2020) 11101.
[31] H. Lian, L. Qi, J. Luo, R. Zhang, K. Hu, Uniform droplet printing of graphene micro-rings based on multiple droplets overwriting and coffee-ring effect, Appl. Surf. Sci. 499 (2020) 143826.
[32] Z. Liu, Y. Yan, Experimental investigation of deposition patterns of citric acid modified magnetic nanofluids droplet affected by substrate temperatures, Int. J. Therm. Sci. 195 (2024) 108666.
[33] T. Wang, M.A. Roberts, I.A. Kinloch, B. Derby, Inkjet printed carbon nanotube networks: the influence of drop spacing and drying on electrical properties, J. Phys. Appl. Phys. 45 (2012) 315304.
[34] H. Machrafi, C. Minetti, P. Dauby, C.S. Iorio, Self-assembly by multi-drop evaporation of carbon-nanotube droplets on a polycarbonate substrate, Phys. E Low-dimens. Syst. Nanostruct. 85 (2017) 206–213.
[35] V. Gigiberiya, M. Manilo, N. Lebovka, Drying of sessile droplets of binary colloidal aqueous mixtures of carbon nanotubes and platelets of Laponite, Colloids Surf. A Physicochem. Eng. Asp. 680 (2024) 132540.
[36] H. Lian, L. Qi, J. Luo, R. Zhang, J. Niu, Direct printing of graphene terahertz closed-ring resonator array from periodic single droplets via enhanced coffee-ring effect, Carbon 215 (2023) 118485.
[37] F.R. Siddiqui, C.-Y. Tso, H. Qiu, C.Y. Chao, S.C. Fu, Hybrid nanofluid spray cooling performance and its residue surface effects: toward thermal management of high heat flux devices, Appl. Therm. Eng. 211 (2022) 118454.
[38] N.S. Howard, A.J. Archer, D. Sibley, D. Southee, K. Wijayantha, Surfactant control of coffee ring formation in carbon nanotube suspensions, Langmuir 39 (2023) 929–941.
[39] J. Wang, X. Yang, J.J. Klemeš, K. Tian, T. Ma, B. Sunden, A review on nanofluid stability: preparation and application, Renew. Sustain. Energy Rev. 188 (2023) 113854.
[40] K. Alexander, S.S. Gajghate, A.S. Katarkar, A. Majumder, S. Bhaumik, Role of nanomaterials and surfactants for the preparation of graphene nanofluid: a review, Mater. Today: Proc. 44 (2021) 1136–1143.
[41] I.W. Almanassra, A.D. Manasrah, U.A. Al-Mubaiyedh, T. Al-Ansari, Z.O. Malaibari, M.A. Atieh, An experimental study on stability and thermal conductivity of water/CNTs nanofluids using different surfactants: a comparison study, J. Mol. Liq. 304 (2020) 111025.
[42] S.U. Ilyas, S. Ridha, F.A.A. Kareem, Dispersion stability and surface tension of SDS-Stabilized saline nanofluids with graphene nanoplatelets, Colloids Surf. A Physicochem. Eng. Asp. 592 (2020) 124584.
[43] K. Singh, S. Sharma, S.M. Gupta, Synergetic effect of SDS/GA mixture on stability of aqueous CNT nanofluid, World 10 (2022) 95–104.
[44] Cakmak N. Keklikcioglu, The impact of surfactants on the stability and thermal conductivity of graphene oxide de-ionized water nanofluids, J. Therm. Anal. Calorim. 139 (2020) 1895–1902.
[45] K. Wusiman, H. Jeong, K. Tulugan, H. Afrianto, H. Chung, Thermal performance of multi-walled carbon nanotubes (MWCNTs) in aqueous suspensions with surfactants SDBS and SDS, Int. Commun. Heat Mass Tran. 41 (2013) 28–33.
[46] Z. Han, A. Fina, Thermal conductivity of carbon nanotubes and their polymer nanocomposites: a review, Prog. Polym. Sci. 36 (2011) 914–944.
[47] S. Ghosh, W. Bao, D.L. Nika, S. Subrina, E.P. Pokatilov, C.N. Lau, A.A. Balandin, Dimensional crossover of thermal transport in few-layer graphene, Nat. Mater. 9 (2010) 555–558.
[48] K.M. Al Balushi, G. Duursma, P. Valluri, K. Sefiane, D. Orejon, Binary mixture droplet evaporation on microstructured decorated surfaces and the mixed stick–slip modes, Langmuir 39 (2023) 8323–8338.